Free-space propagation of autofocusing Airy vortex beams with controllable intensity gradients

Xu Yan (闫 旭)[1,2,3], Lixin Guo (郭立新)[1,2,3,*], Mingjian Cheng (程明建)[2], and Shuirong Chai (柴水荣)[2]

[1]*State Key Laboratory of Integrated Service Networks, Xidian University, Xi'an 710071, China*
[2]*School of Physics and Optoelectronic Engineering, Xidian University, Xi'an 710071, China*
[3]*School of Electronic Engineering, Xidian University, Xi'an 710071, China*
*Corresponding author: lxguo@xidian.edu.cn

Vortex splitting is one of the main causes of instability in orbital angular momentum (OAM) modes transmission. Recent advances in OAM modes free-space propagation have demonstrated that abruptly autofocusing Airy vortex beams (AAVBs) can potentially mitigate the vortex splitting effect. However, different modes of vortex embedding will affect the intensity gradients of the background beams, leading to changes in the propagation characteristics of vortex beams. This study presents the unification of two common methods of coupling autofocusing Airy beams with vortices by introducing a parameter (m), which also controls the intensity gradients and focusing properties of the AAVBs. We demonstrate that vortex splitting can be effectively reduced by selecting an appropriate value of the parameter (m) according to different turbulence conditions. In this manner, the performance of OAM-based free-space optical systems can be improved.

OCIS codes: 010.1290, 010.1300, 010.1330.
doi: 10.3788/COL201917.040101.

The free-space transfer of high-fidelity orbital angular momentum (OAM) signals over large distances has many applications, such as optical communications[1–3], remote sensing[4–6], and imaging systems[7,8]. OAM in nonlinear optics has been discussed[9]. Recent experimental advances in this field indicate that the technology is ready for operational deployment[10]. However, one major obstacle in the transmission of light beams in free-space is atmospheric turbulence, which induces power fluctuations and phase distortions in transmitted beams. Apart from digital signal processing methods, shaping the phase and amplitude of the light field is an efficient way to boost anti-jamming performance and promote certain desired features during propagation.

An optical vortex is a typical representation of the mode of phase modulation. An important feature of optical vortices is that they carry OAM, which can not only potentially increase channel capacity[11], but also help vortex beams propagate through turbulence with greater capability of anti-jamming than conventional Gaussian beams[12]. Accordingly, researchers coupled various background beams with vortices and attempted to achieve superior information carriers in free-space optical (FSO) communications systems, including Laguerre–Gaussian[13], Bessel–Gaussian vortex[14], Airy vortex beams[15], and so on. For a long time, turbulence effects, such as beam spreading, scintillation, beam wander, and angle-of-arrival fluctuation, have been investigated in detail. In contrast, the effect of vortex splitting on OAM-based FSO communications systems has not been investigated in sufficient detail. Earlier, a numerical study indicated that propagation through bulk optical atmospheric turbulence can lead

to changes in the measured average OAM of an optical field[12]. A pioneering experimental demonstration by Lavery *et al.*[16] suggests that the larger a vortex splitting ratio is, the smaller the measured value of an average OAM. Moreover, Ref. [17] found that vortex splitting occurs early in the turbulent atmosphere link and gets further amplified with incessant aberrations during propagation. Therefore, mitigating turbulence induced by vortex splitting is of great significance for improving the performance of OAM-based FSO links.

Recently, Ref. [18] facilitated new feasible methods to weaken the splitting effect on the FSO link by using abruptly autofocusing light beams. Through a considerable amount of researches[19–26], a good understanding of the propagation dynamics of autofocusing Airy-correlated vortex beams has been achieved. There is a new type of autofocusing beam, named the autofocusing hyper-geometric beam[27], which propagates toward the focus following a trajectory similar to that of a ring-Airy vortex beam. However, after propagating through the focus, the spreading velocity of the first ring radius of the autofocusing hyper-geometric beam is much faster than that of the ring-Airy-correlated vortex beams. Overall, it is clear that each vortex beam has a characteristic feature during propagation because of differences in the intensity and phase gradients that are determined by background beams at a vortex position. Therefore, controlling the intensity and phase gradients of background beams is an important means to study the propagation dynamics of ring-Airy-correlated vortex beams.

However, previous studies have not taken into account the effect of differences in the modes of vortex embedding,

which affects the intensity of background beams. In other words, vortices nested within cross-sectional profiles of identical background beams at the same positions in different manners exhibit different features during propagation. The mode of vortex embedding can be divided into two types: the first was presented by Refs. [19] and [20], in which the intensity distribution of the vortex beam at the transmitter strongly depends on the value of its topological charge; in the second case, the intensity distribution is independent of its topological charge value, presented by Refs. [21–23].

This study investigates the effect of two types of vortex embedding on the propagation properties of autofocusing Airy vortex beams (AAVBs) across a free-space channel. These two modes can be consolidated by introducing the parameter (m) that also can be used as a steering parameter to modulate the holistic intensity gradient and focal features of the AAVB. Based on numerical results, we also provide detailed accounts of the role of m in the propagation of the AAVB through turbulent atmosphere, providing guidelines for the design of an optical vortex communication system.

Two vortices, or more, nested within a wavefront will affect each other during propagation. To investigate in detail the difference in vortex propagation characteristics induced by the difference in nesting modes, only the case of one vortex embedded in the cross-sectional profile of a coherent beam is considered here. We compare two different AAVBs that carry the same OAM information. The first can be described as[19,20]

$$E_1 = \{r \exp[i \cdot \text{sign}(l) \cdot \theta] - r_k \exp[i \cdot \text{sign}(l) \cdot \theta_k]\}^{|l|}$$
$$\times \text{Ai}\left(\frac{r_0 - r}{\omega}\right) \exp\left(a \cdot \frac{r_0 - r}{\omega}\right), \qquad (1)$$

where (r, θ) is the radial coordinate; (r_k, θ_k) denotes the center of the optical vortex; $\text{sign}(\cdot)$ is the sign function; l represents the topological charge of the optical vortex, and its sign determines whether the vorticity is clockwise or counter clockwise; ω, r_0, and a refer to the main ring width, radius, and apodization parameters, respectively; $\text{Ai}(\cdot)$ is the Airy function. In view of convenience and generality, we seeded the center of the single vortex at the coordinate origin. Equation (1) can be simplified as

$$E_1' = \text{Ai}\left(\frac{r_0 - r}{\omega}\right) \exp\left(a \cdot \frac{r_0 - r}{\omega}\right) r^{|l|} \exp(il\theta). \qquad (2)$$

The second is written as[21–23]

$$E_2 = \text{Ai}\left(\frac{r_0 - r}{\omega}\right) \exp\left(a \cdot \frac{r_0 - r}{\omega}\right) \exp(il\theta). \qquad (3)$$

Comparing Eqs. (2) and (3), we can introduce a parameter m $(m \geq 0)$, not only to combine the two equations, but also to control the energy ratio of the primary ring to its subsequent oscillations:

$$E_3 = \text{Ai}\left(\frac{r_0 - r}{\omega}\right) \exp\left(a \cdot \frac{r_0 - r}{\omega}\right) r^m \exp(il\theta). \qquad (4)$$

Implementing Eq. (4) with $l = 3$, the normalized intensity distributions and phase patterns at the input plane for different values of m are illustrated in Fig. 1. In Fig. 1(a), the first $(m = 0)$ and third $(m = 3)$ columns correspond to the intensity and phase distributions of the ring-Airy beams described by Eqs. (2) and (3), respectively. As is clearly shown, with the same OAM information, different modes of vortex embedding change the intensity distributions of background beams. Figure 1(b) shows the normalized radial intensity cross-sections of AAVBs corresponding to Fig. 1(a). An energy ratio is defined as $E_r = I_p / I_{\langle \text{sr} \rangle}$, where I_p is the intensity of the central ring of the ring-Airy vortex beam, and $I_{\langle \text{sr} \rangle}$ is the average intensity of subsequent rings. Obviously, as m increases, E_r decreases, which shows that m can be used as a steering parameter to modulate the holistic intensity gradient of AAVBs. Recently, two effective schemes from Refs. [20] and [28] have been introduced to improve the autofocusing property by reshaping the ring structure of autofocusing Airy beams. Unlike these studies, the role of m in this work is to control the energy distribution between the central ring and its subsequent rings or the holistic intensity gradient of background fields.

The most notable feature of autofocusing Airy beams is the abrupt autofocus. As shown in Fig. 1(a), with $m = 1.6$, 3, and 5, the intensities rapidly decrease for the rings near the center but increase for those far from the center. Thus, during the propagation of these tailored AAVBs to the focal plane, the self-healing effect, which makes the energy flow inwardly, occurs simultaneously. Then, the trajectories of AAVBs change significantly under the combined effects of self-healing and self-focusing, eventually leading to the change of the radius and intensity of the focal spot, as illustrated in Fig. 2. The focus can be estimated by
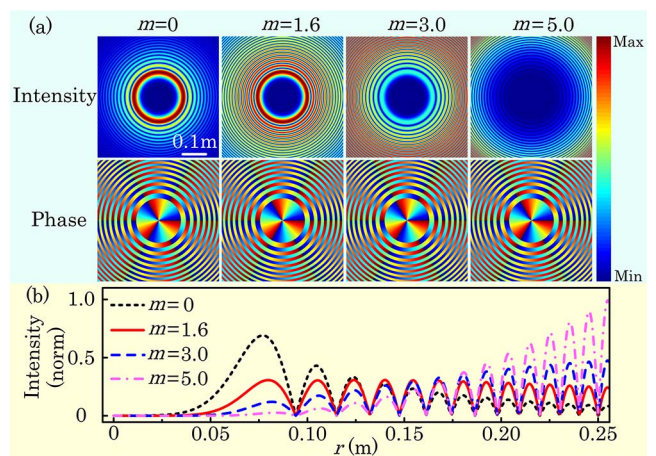

Fig. 1. (a) Intensity and phase distributions of AAVBs for different values of $m = 0$, 1.6, 3, and 5 at the incident plane. (b) Normalized radial intensity plots of (a) in black, red, blue, and purple colors.
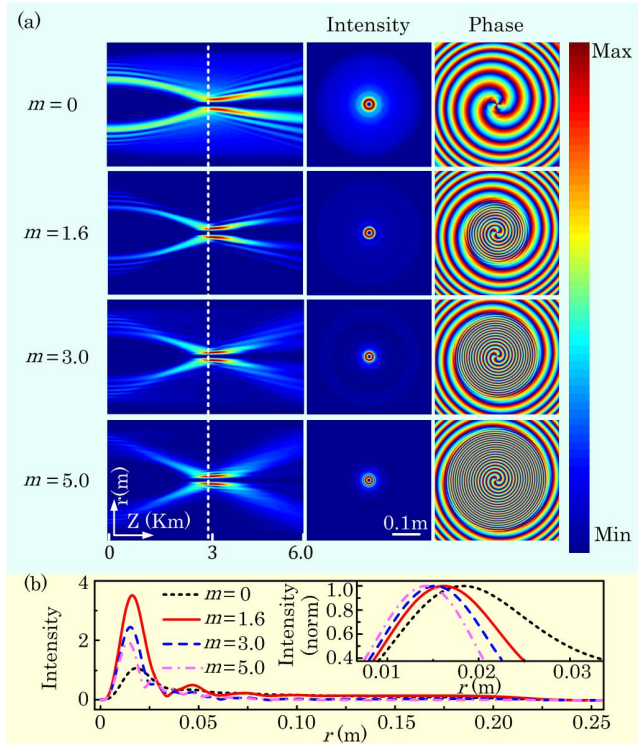
Fig. 2. (a) Free propagating AAVBs with $m = 0$, 1.6, 3, and 5. The side-views of AAVB propagation are given in the first column, and the focal planes are marked by the dashed line. The intensity and phase distributions of AAVBs at the focal plane are given in the second and third columns, respectively. (b) Radial intensity plots of AAVBs at the focal plane in colors. The inset shows normalized intensities, amplifying variations in the radii of the primary rings.

$z = 4\pi\omega^{3/2} r_0^{1/2}/\lambda$[29]. In our simulations, the ring-Airy beam focuses at a position $z = 2.74$ km. The optical fields shown in Fig. 2(a) are calculated by using the beam propagation method[30]. We can clearly see that the intensity feature of AAVB with $m = 0$ follows the well-known parabolic trajectory; whereas, as the value of m increases, the trajectory of AAVB changes significantly. Especially, when $m = 5$, a near-linear intensity trajectory of AAVB is observed before the focal plane. In addition, after the focal plane, the larger the value of m is, the stronger the intensity attenuation and divergence of AAVB are. Figure 2(b) shows the radial intensity distributions of the AAVBs at the focal plane. It can be seen that when $m = 1.6$ and E_r is close to 1, the maximum focal intensity is achieved. Moreover, the inset indicates the normalized intensity plots of Fig. 2(b), clearly showing variations in the radii of the primary rings. As m increases, the radii decrease, suggesting the enhancement of the autofocusing property of the ring-Airy beam. We attribute this result to the fact that, in a linear medium, a vortex moves perpendicularly to the intensity gradient of the background field[31]. In the present study, the gradient of the background field is cylindrically symmetric around the center of the vortex, and thus, the vortex does not experience a displacement in the transverse plane. However, owing to

the additional effects of intensity gradients, the energy of the AAVB flows inward spirally, generating a more elaborate phase structure for itself and shrinking the vortex core size. Unlike the recent work by Jiang et al.[32], in which the abruptly autofocusing property was enhanced by moving the position of peak intensity of the modified circular Airy beam to any ring behind, we change the radius and intensity of the focal spot in the AAVBs by controlling m.

Note that for different main ring widths (r_0) and focus positions (z), m must be modified as well to maintain E_r close to 1 at the incident plane and the maximum intensity at the focal plane.

The propagation of the above ring-Airy beams in turbulent atmosphere was simulated by using a multiple-phase-screen method[33]. As shown in Fig. 3, the free-space propagation and the phase modulation induced by the phase screen are regarded as two processes that are independent and simultaneously completed. The key simulation parameters of this study are given in Table 1.

A recent study[16] indicates that turbulence or any weak noncylindrically symmetric aberration could result in vortex splitting of OAM modes. Vortex splitting can be quantified as $V = \Delta V_{\langle r \rangle}/\omega_0$, where $\Delta V_{\langle r \rangle}$ is the average radial distance from the beam origin for individual vortices, and ω_0 is the beam waist of the transmitted mode[16]. Figure 4 shows examples of four autofocusing Airy OAM modes corresponding to those shown in Fig. 2 after propagating
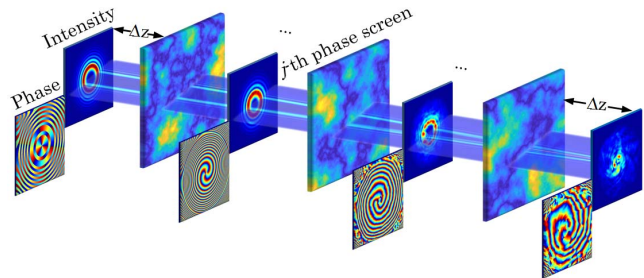

Fig. 3. Multiple random phase screen model.

Table 1. Values of Parameters Used in the Simulations

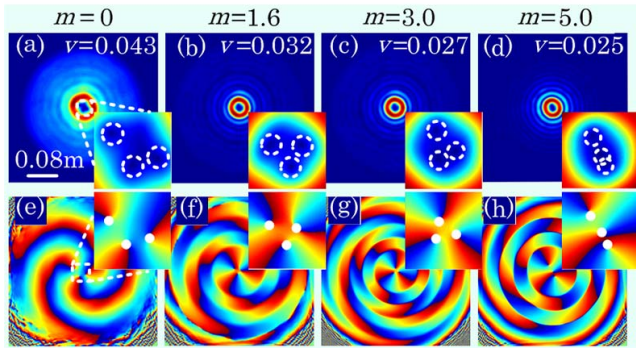| Parameter	Value
Wavelength (λ)	1550 nm
Transverse scales (ω)	0.012 m
Truncation factor (a)	0.1
Grid numbers ($N \times N$)	1024×1024
Sample grid length	5×10^{-4} m
Number of phase screen	50
Turbulence strength (D/r_0)	Varies from 0.96 to 6.6
Inner scale size	0.001 m
Outer scale size	10 m for $D/r_0 \leq 1.67$ and 1 m for $D/r_0 > 1.67$

Fig. 4. (a)–(d) Intensity distributions of AAVBs with $l = 3$ for different values of $m = 0, 1.6, 3$, and 5 after propagation through a turbulent optical channel. (e)–(h) Phase cross-sections of AAVBs corresponding to (a)–(d), respectively. Insets are magnified representations of vortex splitting corresponding to the regions marked by the dashed squares, where phase and intensity patterns of each charge-one vortex are indicated by the overlaid white circles and white dotted circles, respectively.

through turbulent atmosphere with $D/r_0 = 0.42$. It is clear that the topological charge of these vortex beams with $l = 3$ breaks up to give l individual charge-one vortices. During propagation, these individual vortices wander the transverse plane quasi-independently[12], but they are confined to the central ring.

The vortex splitting performance for OAM modes ($l = 3$ and 5) with $m = 0, 1.6, 3$, and 5 under different turbulence conditions at the focal plane is plotted in Fig. 5. For each test run, over 500 simulation samples were averaged. The results show that for lower-order OAM modes (i.e., $l = 3$), the vortex splitting ratio of autofocusing Airy beams decreases as m increases [Fig. 5(a)]. For higher-order OAM modes (i.e., $l = 5$), when $D/r_0 \leq 2.89$, similar to that of $l = 3$, the vortex splitting ratio decreases with m increasing. It is noteworthy that the amount of charge-one vortices is higher at higher topological charges. When the turbulence strength increases, these charge-one vortices will wander the transverse plane much more violently. Owing to the low focal intensity of the central ring for $m = 5$ [Fig. 2(b)], when $D/r_0 > 2.89$, individual vortices cannot be bound, which results in a larger vortex splitting ratio of $m = 5$ than that of $m = 3$. Furthermore, when $D/r_0 > 5.36$, for both $l = 3$ and 5, the topological phase distributions of AAVBs with $m = 3$ and 5 are more severely distorted than those with $m = 0$ and 1.6, hindering the effective transmission of OAM information and preventing the calculation of vortex splitting. We attribute this effect to the two following aspects. (1) Compared with $m = 0$, the cases of $m = 3$ and 5 have smaller light spot sizes, which increases the strength of the beam wander effect. (2) Compared with $m = 1.6$, the cases of $m = 3$ and 5 have lower focal intensity to confine these wandering individual vortices to the central ring, leading to more easily speckled light spots.

In conclusion, we introduce a parameter (m) to control the energy ratio (E_r) and focusing properties of AAVBs
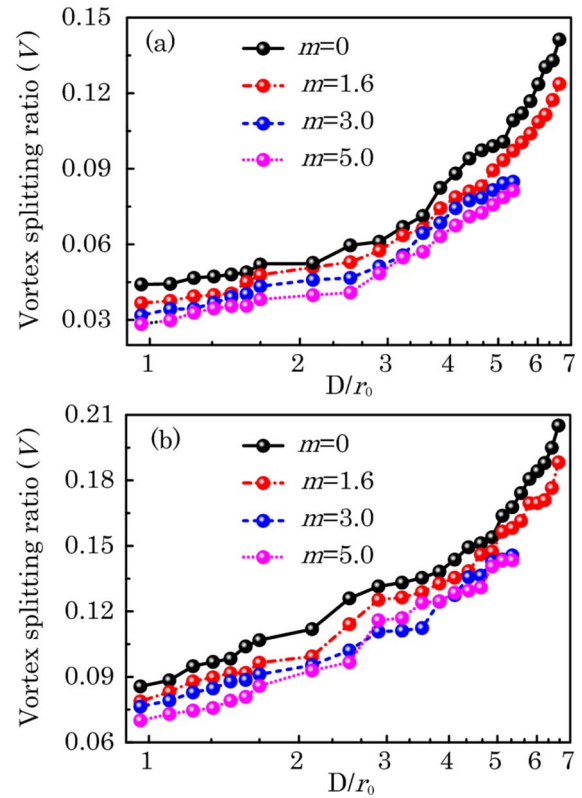

Fig. 5. Plots of vortex splitting ratio (V) as a function of turbulence strength (D/r_0) for (a) $l = 3$ and (b) $l = 5$.

and demonstrate that a proper value of m should be selected for different turbulent strengths to mitigate the vortex splitting effect. Numerical results show that a relatively larger m should be used for weak turbulence (i.e., $D/r_0 \leq 5.36$), and a special value of m should be selected such that E_r close to 1 is maintained for moderate-to-strong turbulence (i.e., $D/r_0 > 5.36$). Furthermore, this work provides new insights into the behavior of AAVBs in turbulence. More importantly, our findings suggest that the implicit intensity modulation induced by differences in the mode of vortex embedding should be taken into account when referring and comparing published studies on the propagation properties of OAM modes, not simply for AAVBs. When implementing this scheme in practice, referring to the prior demonstration in Ref. [22], we can generate AAVBs with $m = 0$ by using an expanded Gaussian beam to illuminate the phase spatial light modulator and utilize a filter to modulate its intensity distribution.

The average OAM value is used as the information carrier in OAM-based communications systems. Therefore, much more work will need to be done to quantify the relation between the average OAM value measured at the receiver and the vortex splitting ratio.

References

1. J. Wang, Chin. Opt. Lett. **15**, 030005 (2017).
2. L. Li, R. Zhang, G. Xie, Y. Ren, Z. Zhao, Z. Wang, C. Liu, H. Song, K. Pang, and R. Bock, Opt. Lett. **43**, 2392 (2018).
3. S. Fu, T. Wang, S. Zhang, Z. Zhang, Y. Zhai, and C. Gao, Photon. Res. **5**, 251 (2017).
4. N. Uribe-Patarroyo, A. Fraine, D. S. Simon, O. Minaeva, and A. V. Sergienko, Phys. Rev. Lett. **110**, 043601 (2013).
5. M. P. Lavery, F. C. Speirits, S. M. Barnett, and M. J. Padgett, Science **341**, 537 (2013).
6. G. Milione, T. Wang, J. Han, and L. Bai, Chin. Opt. Lett. **15**, 030012 (2017).
7. J. Chu, X. Li, Q. Smithwick, and D. Chu, Opt. Lett. **41**, 1490 (2016).
8. K. Liu, Y. Cheng, Z. Yang, H. Wang, Y. Qin, and X. Li, IEEE Antennas Wireless Propag. Lett. **14**, 711 (2015).
9. R. Chen and C. Dai, Nonlinear Dyn. **90**, 1563 (2017).
10. M. Krenn, J. Handsteiner, M. Fink, R. Fickler, R. Ursin, M. Malik, and A. Zeilinger, Proc. Natl. Acad. Sci. U.S.A. **113**, 13648 (2016).
11. A. E. Willner, H. Huang, Y. Yan, Y. Ren, N. Ahmed, G. Xie, C. Bao, L. Li, Y. Cao, and Z. Zhao, Adv. Opt. Photon. **7**, 66 (2015).
12. G. Gbur and R. K. Tyson, J. Opt. Soc. Am. A **25**, 225 (2008).
13. G. Xie, Y. Ren, Y. Yan, H. Huang, N. Ahmed, L. Li, Z. Zhao, C. Bao, M. Tur, S. Ashrafi, and A. E. Willner, Opt. Lett. **41**, 3447 (2016).
14. I. P. Lukin, Appl. Opt. **55**, B61 (2016).
15. H. T. Dai, Y. J. Liu, D. Luo, and X. W. Sun, Opt. Lett. **35**, 4075 (2010).
16. M. P. Lavery, C. Peuntinger, K. Günthner, P. Banzer, D. Elser, R. W. Boyd, M. J. Padgett, C. Marquardt, and G. Leuchs, Sci. Adv. **3**, e1700552 (2017).
17. M. P. J. Lavery, New J. Phys. **20**, 043023 (2018).
18. X. Yan, L. Guo, M. Cheng, and J. Li, Opt. Express **26**, 12605 (2018).
19. Y. Jiang, K. Huang, and X. Lu, Opt. Express **20**, 18579 (2012).
20. B. Chen, C. Chen, X. Peng, Y. Peng, M. Zhou, and D. Deng, Opt. Express **23**, 19288 (2015).
21. Y. Zhu, L. Zhang, and Y. Zhang, Chin. Opt. Lett. **14**, 042101 (2016).
22. P. Li, S. Liu, T. Peng, G. Xie, X. Gan, and J. Zhao, Opt. Express **22**, 7598 (2014).
23. G. Lao, Z. Zhang, and D. Zhao, Opt. Express **24**, 18082 (2016).
24. X. Peng, Y. Peng, D. Li, L. Zhang, J. Zhuang, F. Zhao, X. Chen, X. Yang, and D. Deng, Opt. Express **25**, 13527 (2017).
25. Y. Zhu, Y. Zhang, and Z. Hu, Opt. Express **24**, 10847 (2016).
26. B. Wei, S. Liu, P. Chen, S. Qi, Y. Zhang, W. Hu, Y. Lu, and J. Zhao, Appl. Phys. Lett. **112**, 121101 (2018).
27. A. A. Kovalev, V. V. Kotlyar, and A. P. Porfirev, J. Opt. **18**, 025610 (2016).
28. N. Li, Y. Jiang, K. Huang, and X. Lu, Opt. Express **22**, 22847 (2014).
29. P. Panagiotopoulos, D. G. Papazoglou, A. Couairon, and S. Tzortzakis, Nat. Commun. **4**, 3622 (2013).
30. M. S. Wartak, *Computational Photonics: An Introduction with MATLAB* (Cambridge University, 2013).
31. D. Rozas, C. Law, and G. Swartzlander, J. Opt. Soc. Am. B **14**, 3054 (1997).
32. Y. Jiang, X. Zhu, W. Yu, H. Shao, W. Zheng, and X. Lu, Opt. Express **23**, 29834 (2015).
33. J. D. Schmidt, *Numerical Simulation of Optical Wave Propagation with Examples in MATLAB* (SPIE, 2010).